

<sub>1</sub> Study of neutrino-nucleus interaction at around 1 GeV using  
<sub>2</sub> cuboid lattice neutrino detector, WAGASCI, muon range  
<sub>3</sub> detectors and magnetized spectrometer, Baby MIND, at  
<sub>4</sub> J-PARC neutrino monitor hall

<sub>5</sub> A. Bonnemaison, R. Cornat, L. Domine, O. Drapier, O. Ferreira, F. Gastaldi,  
<sub>6</sub> M. Gonin, J. Imber, M. Licciardi, F. Magniette, T. Mueller, L. Vignoli, and O. Volcy  
<sub>7</sub> *Ecole Polytechnique, IN2P3-CNRS, Laboratoire Leprince-Ringuet, Palaiseau,*  
<sub>8</sub> *France*

<sub>9</sub> S. Cao and T. Kobayashi

<sub>10</sub> *High Energy Accelerator Research Organization (KEK), Tsukuba, Ibaraki, Japan*

<sub>11</sub> M. Khabibullin, A. Khotjantsev, A. Kostin, Y. Kudenko, A. Mefodiev, O. Mineev,  
<sub>12</sub> S. Suvorov, and N. Yershov

<sub>13</sub> *Institute for Nuclear Research of the Russian Academy of Sciences, Moscow, Russia*

<sub>14</sub> B. Quilain

<sub>15</sub> *Kavli Institute for the Physics and Mathematics of the Universe (WPI), The*  
<sub>16</sub> *University of Tokyo Institutes for Advanced Study, University of Tokyo, Kashiwa,*  
<sub>17</sub> *Chiba, Japan*

<sub>18</sub> T. Hayashino, A. Hiramoto, A.K. Ichikawa, K. Nakamura, T. Nakaya, K Yasutome,  
<sub>19</sub> and K. Yoshida

<sub>20</sub> *Kyoto University, Department of Physics, Kyoto, Japan*

<sub>21</sub> Y. Azuma, J. Harada, T. Inoue, K. Kin, N. Kukita, S. Tanaka, Y. Seiya,  
<sub>22</sub> K. Wakamatsu, and K. Yamamoto

<sub>23</sub> *Osaka City University, Department of Physics, Osaka, Japan*

24 A. Blondel, F. Cadoux, Y. Favere, E. Noah, L. Nicola, and S. Parsa

25 *University of Geneva, Section de Physique, DPNC, Geneva, Switzerland*

26 N. Chikuma, F. Hosomi, T. Koga, R. Tamura, and M. Yokoyama

27 *University of Tokyo, Department of Physics, Tokyo, Japan*

28 Y. Hayato

29 *University of Tokyo, Institute for Cosmic Ray Research, Kamioka Observatory,  
30 Kamioka, Japan*

31 Y. Asada, K. Matsushita, A. Minamino, K. Okamoto, and D. Yamaguchi

32 *Yokohama National University, Faculty of Engineering, Yokohama, Japan*

33 December 14, 2017

34 **Abstract**

35 We, the WAGASCI collaboration, proposes to perform the study of the neutrino-  
36 nucleus interaction at the B2 floor of the neutrino monitor building with a new-type  
37 fine-grained neutrino detector and muon range detectors. The hollow cuboid lattice  
38 scintillators filled with water as the neutrino interaction target (known as WAGASCI  
39 module) would enable the measurement of cross section on  $H_2O$ . Measurement in wide  
40 phase space becomes possible by the combination of the WAGASCI modules and side-  
41 and downstream- muon range detectors (MRD's). The downstream-MRD, so called  
42 the Baby MIIND detector, also works as a magnet and provides the charge identification  
43 capability as well as magnetic momentum measurement for high energy muons. The  
44 nominal experimental setup has two WAGASCI modules. Most of the detectors have  
45 already been constructed and have been commissioned in the J-PARC T59 experiment  
46 and the CERN neutrino platform and the collaboration will be ready to proceed to  
47 the physics data taking by January 2019. The experiment can run parasitically with  
48 T2K, without dedicated beam time. With one-year data taking (roughly  $5 \times 10^{20}$   
49 POT) in neutrino-mode and another one-year in antineutrino mode, expected numbers  
50 of charged-current interaction event are 5,400 and 2,240 for one WAGASCI module.  
51 respectively. We will provide the inclusive and exclusive differential cross sections of the  
52 charged current neutrino and antineutrino interactions on water and hydrocarbon with  
53 slightly higher neutrino energy than T2K ND280 with wider angler acceptance. By  
54 combining our measurements with those from ND280, model-independent extraction

55 of the cross section for narrow energy spread becomes possible. These measurements  
56 would improve the understanding of the neutrino-nucleus interaction at around 1 GeV  
57 and also contribute to reducing one of the most significant uncertainties of the T2K  
58 experiment.

## 59 **Contents**

60	<b>1</b>	<b>Introduction</b>	<b>4</b>
61	<b>2</b>	<b>Experimental Setup</b>	<b>5</b>
62	2.1	WAGASCI modules . . . . .	5
63	2.1.1	Detector . . . . .	5
64	2.1.2	Electronics . . . . .	7
65	2.1.3	Water system . . . . .	9
66	2.2	INGRID Proton module . . . . .	10
67	2.3	Baby MIND . . . . .	11
68	2.3.1	Magnet modules . . . . .	12
69	2.3.2	Scintillator modules . . . . .	13
70	2.3.3	Electronics . . . . .	15
71	2.3.4	Pefromance check . . . . .	16
72	2.4	Side muon range detector . . . . .	17
73	<b>3</b>	<b>Physics goals</b>	<b>19</b>
74	3.1	Expected number of events . . . . .	20
75	3.2	Pseudo-monochromatic beam by using different off-axis fluxes . . . . .	20
76	3.3	Extraction of Cross sections . . . . .	20
77	3.4	Subjects WAGASCI can contribute . . . . .	22
78	<b>4</b>	<b>Status of J-PARC T59 experiment</b>	<b>24</b>
79	<b>5</b>	<b>MC studies</b>	<b>26</b>
80	5.1	Simulation setup . . . . .	26
81	5.2	Charged-current event selection . . . . .	27
82	5.3	Standalone WAGASCI-module tracking performance . . . . .	30
83	5.3.1	Expected performance of the water-in WAGASCI module . . . . .	31
84	5.3.2	Expected performance of the water-out WAGASCI module . . . . .	33
85	<b>6</b>	<b>Schedule</b>	<b>35</b>
86	<b>7</b>	<b>Requests</b>	<b>35</b>
87	7.1	Neutrino beam . . . . .	35
88	7.2	Equipment request including power line . . . . .	35

89    **1 Introduction**

90    The understanding of neutrino-nucleus interactions in the 1 GeV energy region is critical  
91    for the success of accelerator-based neutrino oscillation experiments such as the T2K exper-  
92    iment. Complicated multi-body effects of nuclei render this understanding difficult. The  
93    T2K near detectors have been measuring these and significant progress has been achieved.  
94    However, the understanding is still limited. One of the big factors preventing a complete  
95    understanding is the non-monochromatic neutrino beam spectrum. Measurements with  
96    distinct but partially overlapping beam spectra would be a great benefit in resolving the  
97    contribution from different neutrino energies. We, the WAGASCI collaboration, proposes  
98    to study the neutrino-nucleus interaction at the B2 floor of the neutrino monitor build-  
99    ing, where different neutrino spectra from the T2K off-axis near detector (ND280) can  
100   be obtained due to the different off-axis position. Our experimental setup contains two  
101   hollow cuboid lattice detectors filled with water as the neutrino interaction target (known  
102   as WAGASCI modules), two side- and one downstream- muon range detectors(MRD's).  
103   We will have two types of the WAGASCI modules, a water-in module and a water-out  
104   module. The water-in WAGASCI module has water the hollow cuboid lattice, and the  
105   water-out WAGASCI module doesn't have water inside the lattice. The hollow cuboid  
106   lattice and side-MRD's allow a measurement of wider-angle scattering than ND280. High  
107   water to scintillator material ratio enables the measurement of the neutrino interaction  
108   with water, which is highly desired for the T2K experiment because it's far detector,  
109   Super-Kamiokande, is composed of water. The MRD's consist of plastic scintillators and  
110   iron plates. The downstream-MRD, so called the Baby MIND detector, also works as a  
111   magnet and provides the charge identification capability as well as magnetic momentum  
112   measurement for high energy muons. The charge identification is essentially important to  
113   select antineutrino events in the antineutrino beam because contamination of the neutrino  
114   events is as high as 30%. Most of the detectors have already been constructed. The WA-  
115   GASCI modules have been commissioned as the J-PARC T59 experiment and the Baby  
116   MIND detector was commissioned at the CERN neutrino platform. Therefore, the collabo-  
117   ration will be ready to proceed to the physics data taking by January 2019. We will provide  
118   the cross sections of the charged current neutrino and antineutrino interactions on water  
119   with slightly higher neutrino energy than T2K ND280 with wide angler acceptance. The  
120   requested beam time is one-year in neutrino-mode and another one-year in antineutrino  
121   mode assuming that the POT for the fast extraction in each year is more than  $5 \times 10^{20}$  POT.  
122   When combined with ND280 measurements, our measurement would greatly improve the  
123   understanding of the neutrino interaction at around 1 GeV and contribute to reducing one  
124   of the most significant uncertainties of the T2K experiment.

125 **2 Experimental Setup**

126 Figure 1 and 2 show a schematic view and a CAD drawing of the entire set of detectors.  
127 Central neutrino target detectors consist of two WAGASCI modules and T2K INGRID  
128 proton module. Inside the WAGASCI module, plastic scintillator bars are aligned as a  
129 hollow cuboid lattice and spaces in the lattice are filled with water for a water-in WAGASCI  
130 module. T2K INGRID proton module is a full active neutrino target detector which is  
131 composed only with scintillator bars in its tracking region. The central detectors are  
132 surrounded by two side- and one downstream- muon range detectors(MRD's) The MRD's  
133 are used to select muon tracks from the charged-current (CC) interactions and to reject  
134 short tracks caused by neutral particles that originate mainly from neutrino interactions in  
135 material surrounding the central detector, like the walls of the detector hall, neutrons and  
136 gammas, or neutral-current (NC) interactions. The muon momentum can be reconstructed  
137 from its range inside the detector. The MRD's consist of plastic scintillators and iron plates.  
138 The downstream-MRD, also known as the Baby MIND detector, additionally has a coil  
139 wound around each of the iron plates so it may be magnetized. This provides the charge  
140 selection capability.

141 For all detectors, scintillation light in the scintillator bar is collected and transported  
142 to a photodetector with a wavelength shifting fiber (WLS fiber). The light is read out by  
143 a photodetector, Multi-Pixel Photon Counter (MPPC), attached to one end of the WLS  
144 fiber. The signal from the MPPC is read out by the dedicated electronics developed for  
145 the test experiment to enable bunch separation in the beam spill. The readout electronics  
146 are triggered using the beam-timing signal from MR to synchronize to the beam. The  
147 beam-timing signal is branched from those for T2K, and will not effect T2K data taking.

148 T2K adopted the off-axis beam method, in which the neutrino beam is intentionally  
149 directed 2.5 degrees away from SK producing a narrow band  $\nu_\mu$  beam. The off-axis near  
150 detector, ND280, is installed towards the SK direction in the B1 floor of the near detector  
151 hall of the J-PARC neutrino beam-line. We propose to install our detector in the B2 floor  
152 of the near detector hall, where the off-axis angle of 1.5 degrees is slightly different to the  
153 2.5 degrees of ND280. The candidate detector position in the B2 floor is shown in Figure  
154 3. The expected neutrino energy spectrum at the candidate position is shown in Figure 4.

155 **2.1 WAGASCI modules**

156 **2.1.1 Detector**

157 The WAGASCI modules are mainly composed of 1280 plastic scintillator bars and a sur-  
158 rounding stainless steel tank as shown in Figure 5. The total number of channels in one  
159 WAGASCI module is 1280. The stainless steel tank is constructed by welding stainless  
160 steel plates, is sized as 460mm×1250mm×1250 mm, and weighs 0.5 tonne.

161 One WAGASCI module consists of 16 scintillator tracking planes, where each plane  
162 is an array of 80 scintillator bars fixed with ABS frames. The 40 bars, called parallel

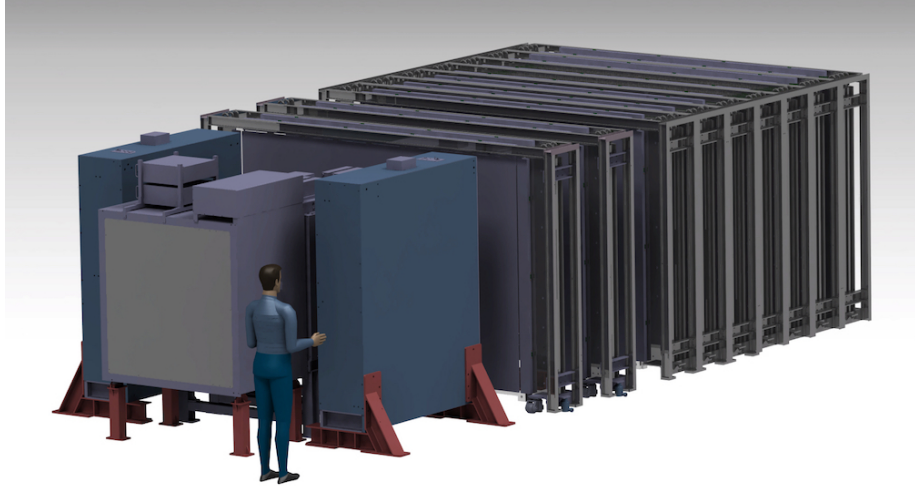


Figure 1: Schematic view of entire sets of detectors.

163 scintillators, are placed perpendicularly to the beam, and the other 40 bars, called lattice  
 164 scintillators, are placed in parallel to the beam with hollow cuboid lattice in the tracking  
 165 plane as shown in Figure 5. Thanks to the hollow cuboid lattice of the scintillator bars,  
 166 the WAGASCI module has  $4\pi$  angular acceptance for charged particles.

167 Thin plastic scintillator bars produced at Fermilab by extrusion method, mainly consists  
 168 of polystyrene and are surrounded by thin reflector including  $\text{TiO}^2$  (3 mm in thickness)  
 169 are used for the WAGASCI modules to reduce the mass ratio of scintillator bars to water,  
 170 because neutrino interactions in the scintillator bars are a background for the cross section  
 171 measurements on  $\text{H}_2\text{O}$ . Each scintillator bar is sized as 1020mm×25mm×3 mm including  
 172 the reflector part, and half of all the scintillator bars have 50-mm-interval slits to form the  
 173 hollow cuboid lattice (Figure 6 ).

174 We will have two types of the WAGASCI modules, a water-in module and a water-out  
 175 module. The water-in WAGASCI module has water in spaces of the hollow cuboid lattice.  
 176 The total water mass serving as neutrino targets in the fiducial volume of the module is  
 177 188 kg, and the mass ratio of scintillator bars to water is 80 %. The water-out WAGASCI  
 178 module doesn't have water inside the detector. The total CH mass serving as neutrino  
 179 target in the fiducial volume of the module is 47 kg, and the mass fraction of scintillator  
 180 bars is 100 %.

181 Scintillation light is collected by wave length shifting fibers, Y-11 (non-S type with a  
 182 diameter of 1.0 mm produced by Kuraray. A fiber is glued by optical cement in a groove  
 183 on surface of a scintillator bar. 32 fibers are gathered together by a fiber bundle at edge  
 184 of the module, and lead scintillation light to a 32-channel arrayed MPPC. Since crosstalk

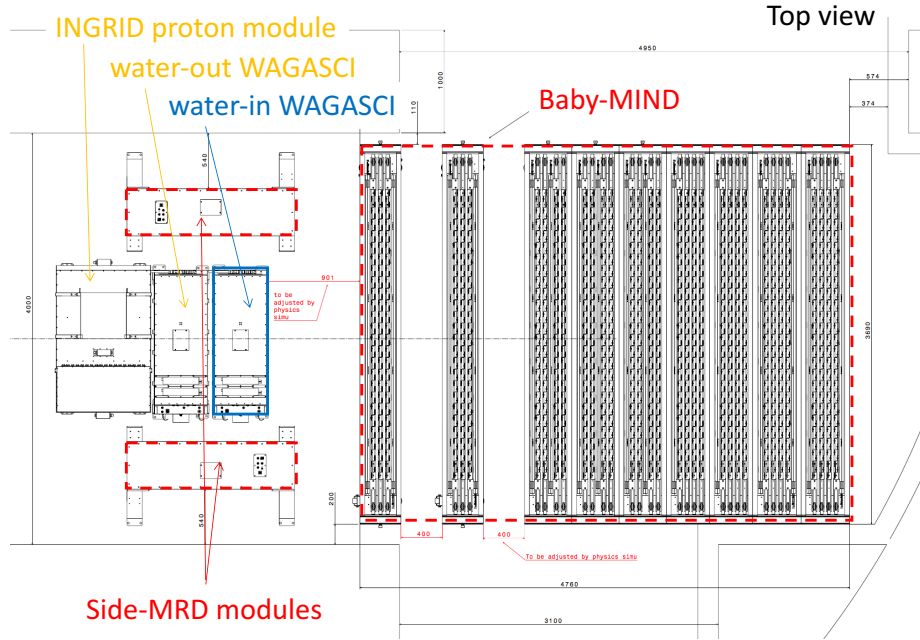


Figure 2: Top view of entire sets of detectors.

of light yield due to reflection on the inner surface of each cell has been observed, all the scintillator bars are painted black by aqueous color spray. It is confirmed by measurements with cosmic rays that black painting on the surface of the scintillator bars suppresses this crosstalk so that no significant crosstalk effect is observed within uncertainty.

32-channel arrayed MPPCs, as shown in the Figure 7, are used for the modules. The surface of the fiber bundle is polished and directly attached onto the 32-channel arrayed MPPCs. The positions of 32 fibers on the bundle are aligned to fit the channels of MPPCs. The MPPC is a product of Hamamatsu Photonics, S13660(ES1), with suppressed noise rate of  $\sim$ 6 kHz per channel at 0.5 p.e. threshold. For each MPPC channel, 716 pixels of APD are aligned in a shape of circle.

195 2.1.2 Electronics

196 As front-end electronics of this detector, a Silicon PM Integrated Read-Out Chip (SPIROC)  
 197 [13] is adopted. SPIROC is a 36-channel auto-triggered front-end ASIC, and is produced  
 198 by OMEGA/ IN2P3. It not only contains an analog signal processing part such as amplifi-  
 199 cation and shaping of the waveform, but contains a digital signal processing parts such as  
 200 auto-trigger and timing measurement. Charge of MPPC signal is sampled by track-and-

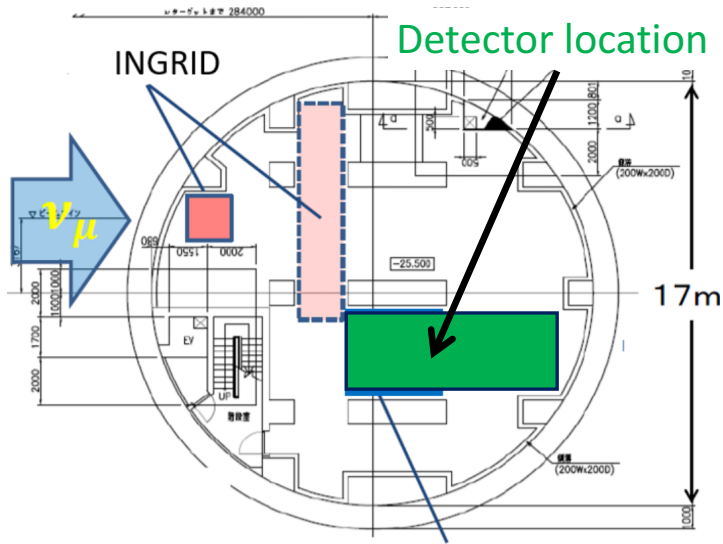


Figure 3: Candidate detector position on the B2 floor of the near detector hall.

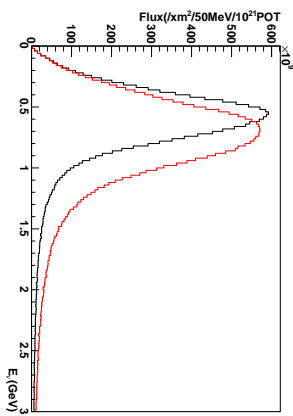


Figure 4: Neutrino energy spectrum at the candidate detector position(red, off-axis 1.5 degree). The spectrum at the ND280 site (black, off-axis 2.5 degree) is also shown.

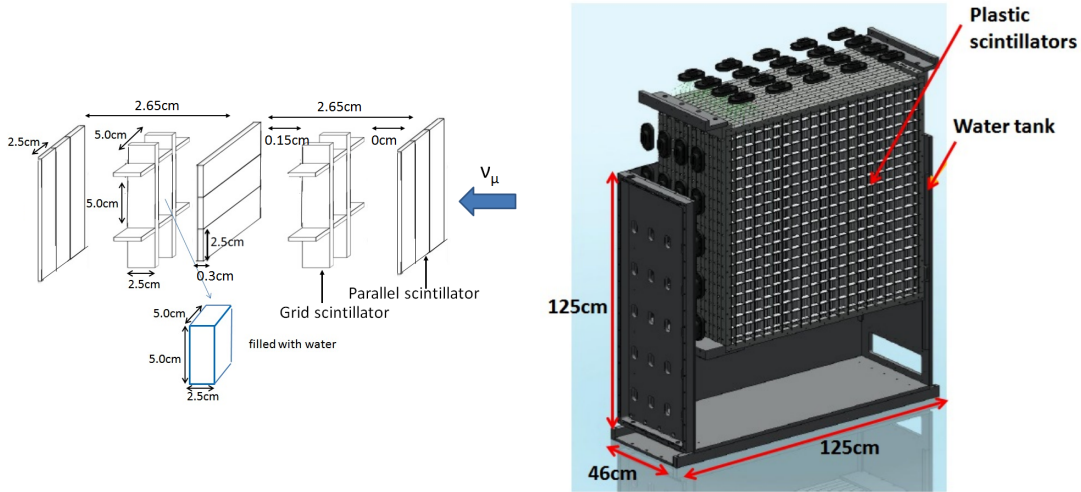


Figure 5: Schematic views of hollow cuboid lattice of plastic scintillator bars (left) and WAGASCI module (right).

hold circuit. A Front-end electronics board, Active Sensor Unit (ASU), has been developed with the SPIROC2D chip, which is the latest version of SPIROC. Each readout board is designed to control a 32-channel arrayed MPPC, and 40 of the ASU boards are aligned on the module surface. The data acquisition system used for this detector, including back-end boards, has been developed for prototypes of ultra-granular calorimeters for the International Linear Collider (ILC) [6], and independent of the T2K DAQ system. To synchronize the DAQ system to J- PARC neutrino beam, pre-beam trigger and beam trigger are sent to the clock control card. The beam trigger signals are converted from optical signals to NIM signals at NIM module on the B2 floor. In addition, the information of spill number are delivered with 16-bit ECL level signals, and converted to an Ethernet frame by an FPGA evaluation board to be directly sent to the DAQ PC. The electronics readout scheme is shown in Figure 8.

### 2.1.3 Water system

Pure water is filled to the water tank of the water-in WAGASCI module as follows. First, the water storage tank located at the B2 floor of the NM pit is filled with water delivered from a water tap on the ground level through a long hose. Second, the water is pumped to the other water storage tank though a water filler to produce pure water. Third, a compound preservative called Germall plus, which is the same preservative used in one of the sub-detectors of T2K ND280, FGD2, is put into the water to keep water from being bad. Then, the water is poured to the water-in WAGASCI module, and it is kept in the

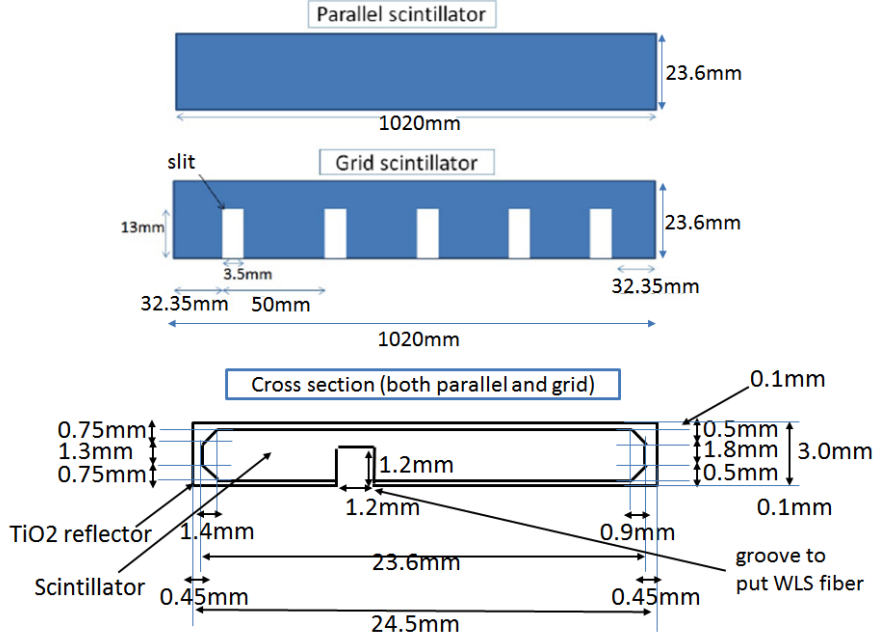


Figure 6: Geometry of scintillators used for WAGASCI modules.

221 module during the neutrino beam operation and not to be circulated.

## 222 2.2 INGRID Proton module

223 INGRID Proton module is a neutrino detector of the T2K experiment. It is a fully-active  
 224 tracking detector which consists of only scintillator strips. The purpose of this Proton  
 225 Module is to separate the neutrino interaction types by detecting the protons and pions  
 226 together with the muons from the neutrino interactions, and to measure the neutrino cross  
 227 section for each interaction type. It consists of 36 tracking planes surrounded by veto  
 228 planes (Figure 9), where each tracking plane is an array of two types of scintillator strips.  
 229 The 16 strips in the inner region have dimensions of  $25\text{mm} \times 13\text{mm} \times 1200\text{mm}$ , while the 16  
 230 strips in the outer region have dimensions of  $50\text{mm} \times 10\text{mm} \times 1200\text{mm}$ , making a plane of  
 231  $1200\text{mm} \times 1200\text{mm}$  in the horizontal and vertical directions. The former is the scintillator  
 232 produced for the K2K SciBar detector [4] and the latter was produced for INGRID. The  
 233 tracking planes are placed perpendicular to the beam axis at 23mm intervals. Since the  
 234 strips are aligned in one direction, each tracking plane is sensitive to either the horizontal or  
 235 vertical position of the tracks. The tracking planes are therefore placed alternating in the  
 236 horizontal and vertical directions so that three-dimensional tracks can be reconstructed.  
 237 The tracking planes also serve as the neutrino interaction target. As with the WAGASCI

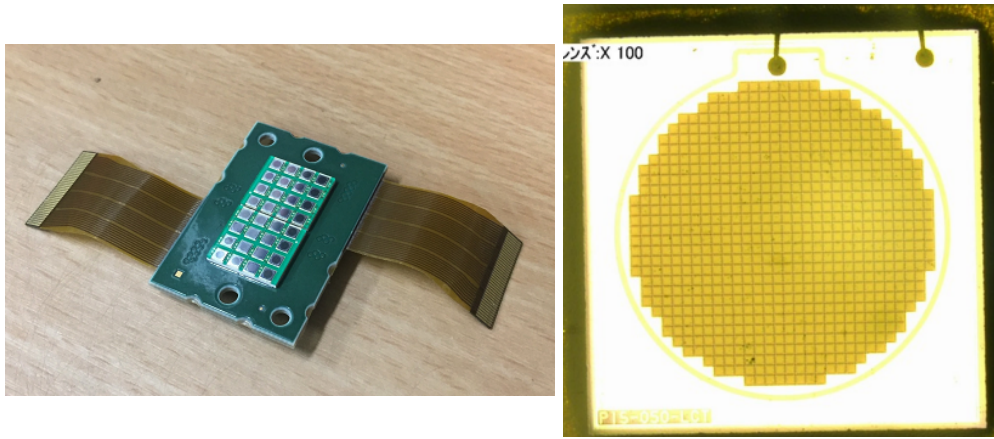


Figure 7: 32-channel arrayed MPPC (left) and an enlarged view of one MPPC channel (right).

238 modules, scintillation light is read out by a WLS fiber and MPPC.

239 It was installed on the neutrino beam axis on the SS floor of the T2K near detector hall  
 240 in 2010, and had been used for neutrino cross section measurements. In August 2017, it  
 241 was moved to the B2 floor of the T2K near detector hall by J-PARC T59 after getting the  
 242 approval from T2K to use them. J-PARC T59 is performing a neutrino beam measurement  
 243 using the detector from October 2017, and the measurement will continue until May 2018  
 244 as we will discuss in Sec. 4.

245 We will operate the INGRID Proton module using the T2K near detector electronics/  
 246 DAQ system in the same way as J-PARC T59. A proposal to use the module and its  
 247 electronics for our project will be submitted to the T2K collaboration.

### 248 2.3 Baby MIND

249 The Baby MIND is the downstream Muon Range Detector. It also works as a magnet and  
 250 provides the charge identification capability as well as magnetic momentum measurement  
 251 for high energy muons.

252 The Baby MIND collaboration<sup>1</sup> submitted a proposal to the SPSC at CERN, SPSC-P-  
 253 353. The project was approved by the CERN research board as Neutrino Platform project  
 254 NP05 and constructed. The detector consists of 33 magnet modules, each 3500 mm ×  
 255 2000 mm × 50 mm (30 mm steel) with a mass of approximately 2 tonnes. Of these magnet  
 256 modules, 18 are instrumented with plastic scintillator modules.

---

<sup>1</sup>Contact person: E. Noah, Spokesperson: A. Blondel, Deputy spokesperson: Y. Kudenko

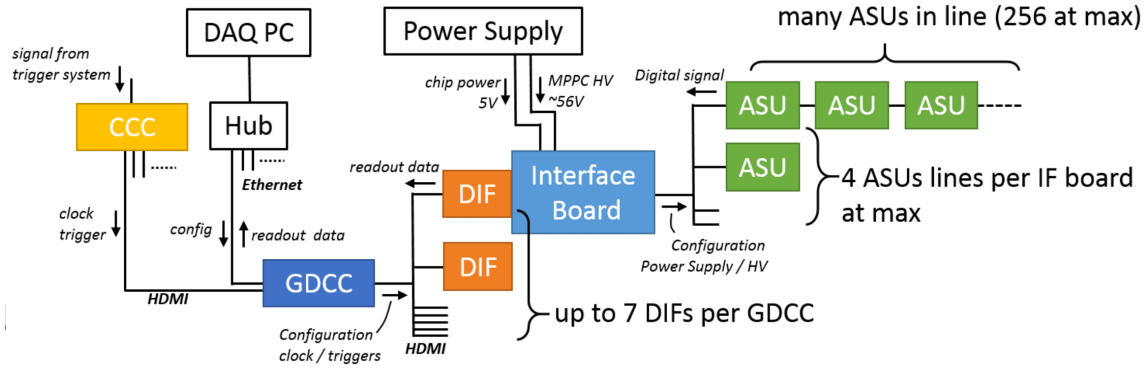


Figure 8: WAGASCI electronics readout scheme.

### 2.3.1 Magnet modules

Traditional layouts for magnetized iron neutrino detectors (e.g. MINOS) tend to be monolithic blocks with a unique pitch between consecutive steel segments and large conductor coils threaded around the whole magnet volume. The Baby MIND detector, like traditional designs, is built from sheets of iron interleaved with scintillator detector modules. However Baby MIND is novel in that the iron segments are all individually magnetized as shown in Figure 10, allowing for far greater flexibility in the setting of the pitch between segments, and in the allowable geometries that these detectors can take.

The key design outcome is a highly optimized magnetic field map. A double-slit configuration for coil winding was adopted to increase the area over which the magnetic flux lines are homogeneous in  $B_x$  across the central tracking region. Simulations show the magnet field map to be very uniform over this central tracking region covering an area of  $2800 \times 2000 \text{ mm}^2$ , Figure 11. The  $B_x$  component dominates in this region, with negligible  $B_y$  and  $B_z$ . This was confirmed by measuring the field with 9 pick-up coils wound around the first module. Subsequent modules were equipped with one pick-up coil. Test results on the 33 modules show all achieve the required field of 1.5 T for a current of 140 A, with a total power consumption of 11.5 kW. The polarity of the field map shown in Figure 11 (middle) can be reversed by changing the power supply configuration.

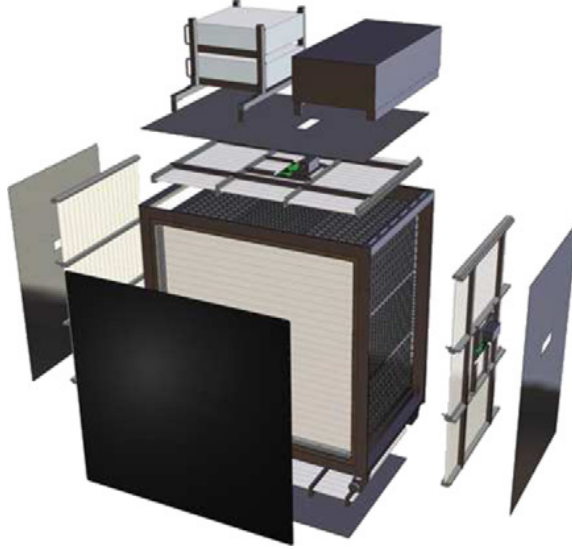


Figure 9: Schematic view of INGRID Proton module.

275 **2.3.2 Scintillator modules**

276 Each of the 18 scintillator modules is constructed from 2 planes of horizontal counters (95  
 277 counters in total) and 2 planes of vertical counters (16 counters in total) [3], arranged  
 278 with an overlap between planes to achieve close to 100% hit efficiency for minimum ionizing  
 279 muons. The arrangement of planes within a module is vertical-horizontal-horizontal-  
 280 vertical. This arrangement was the result of an assembly approach whereby each plane  
 281 was built from 2 half-planes, with each half plane consisting of a horizontal plane and a  
 282 vertical plane. The scintillator bars are held in place using structural ladders that align  
 283 and maintain the counters, Figure 12. No glue is used in the process, so counters can be  
 284 replaced. Aluminum sheets front and back provide light tightness.

285 The plastic scintillator counters were made from 220 mm-wide slabs, consisting of  
 286 extruded polystyrene doped with 1.5% paraterphenyl (PTP) and 0.01% POPOP. They were  
 287 cut to size then covered with a 30-100  $\mu\text{m}$  thick diffuse reflector resulting from etching of the  
 288 surface with a chemical agent [10, 11]. The horizontal counter size is  $2880 \times 31 \times 7.5 \text{ mm}^3$ ,  
 289 with one groove along the length of the bar in which sits a wavelength shifting fiber from  
 290 Kuraray. The vertical counter size is  $1950 \times 210 \times 7.5 \text{ mm}^3$ , with one U-shaped groove  
 291 along the bar. On each counter, two custom connectors house silicon photomultipliers,  
 292 MPPC type S12571-025C from Hamamatsu, either side of the horizontal counter, and  
 293 both connectors at the top for the vertical counter. This geometrical configuration for  
 294 vertical counters was chosen for ease of connectivity to the electronics, and maintenance  
 295 operations.

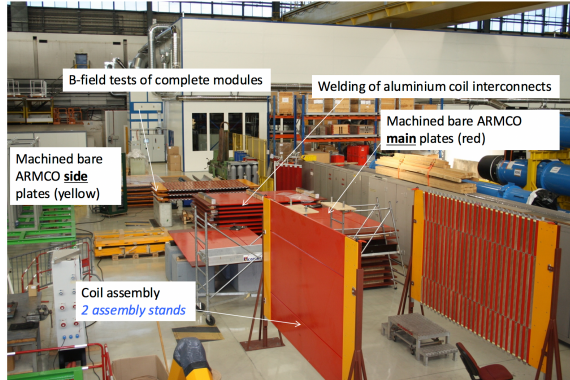


Figure 10: Magnet assembly zone at CERN.

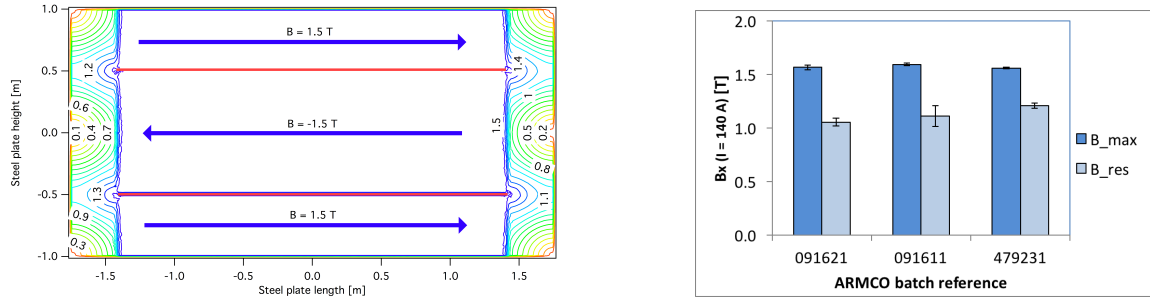


Figure 11: Left) Magnetic field map with a coil along 2800 mm of the length of the plate.  
Right) Measured B field for 33 modules.



Figure 12: Scintillator modules assembly. Left) top of front half-module showing vertical counters, and the spacer-ladders that set the pitch between horizontal counters and hold them in place. Middle) rear half-module showing horizontal counters on their ladders. Right) Assembled rear half-module, the front half-module can be seen in the background.

296 A total of 1744 horizontal counters and 315 vertical counters (including spares) were  
297 produced at the Uniplast company (Vladimir, Russia).

### 298 2.3.3 Electronics

The Baby MIND electronic readout scheme includes several custom-designed boards [12]. The revised version is shown in Figure 13. At the heart of the system is the electronics Front End Board (FEB), developed by the University of Geneva. The readout system includes two ancillary boards, the Backplane, and the Master Clock Board (MCB) whose development has been managed by INRNE (Bulgarian Academy of Sciences) collaborators.

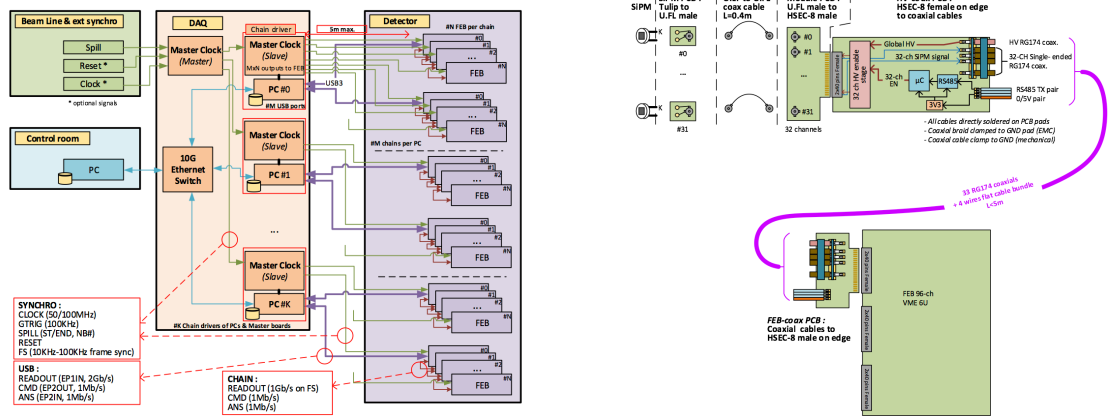


Figure 13: Left) Baby MIND electronics readout scheme. Right) SiPM-to-FEB connectivity.

The FEBv2 hosts 3 CITIROC chips that can each read in signals from 32 SiPMs [7]. Each signal input is processed by a high gain (HG), and a separate low gain (LG), signal path. The outputs from the slow shapers can be sampled using one of two modes: a mode with an externally applied delay, and a peak detector mode. A faster shaper can be switched to either HG or LG paths, followed by discriminators with adjustable thresholds providing 32 individual trigger outputs and one OR32 trigger output. An Altera ARIA5 FPGA on the FEBv2 samples these trigger outputs at 400 MHz, recording rising and falling times for the individual triggers and assigning time stamps to these. Time-over-threshold, the difference between falling and rising times, gives some measure of signal amplitude. This is used in addition to charge information and proves useful if there is more than one hit per bar within the  $\sim 9 \mu\text{s}$  deadtime due to the readout of the multiplexed charge output. The ARIA5 also manages the digitization of the sampled CITIROC multiplexed HG and LG outputs via a 12-bit 8-ch ADC.

317 The internal 400 MHz clock on the FEBv2 can be synchronized to a common 100 MHz  
318 clock. The synchronization subsystem combines input signals from the beam line into

319 a digital synchronization signal (SYNC) and produces a common detector clock (CLK)  
 320 which can eventually be synchronised to an external experiment clock. Both SYNC and  
 321 CLK signals are distributed to the FEBs. Tests show the FEB-to-FEB CLK(SYNC) delay  
 322 difference to be 50 ps (70 ps). Signals from the beam line at WAGASCI include two  
 323 separate timing signals, arriving 100 ms and 30  $\mu$ s before the neutrino beam at the near  
 324 detectors. The spill number is available as a 16-bit signal.

### 325 2.3.4 Pefromance check

326 All counters were measured at INR Moscow with a cosmic ray setup using the same type  
 327 S12571-025C MPPCs and a CAEN DT5742 digitizer. The average light yield (sum from  
 328 both ends) was measured to be 37.5 photo-electrons (p.e.) per minimum ionizing particle  
 329 (MIP) and 65 p.e./MIP for vertical and horizontal counters, respectively. After shipment  
 330 to CERN, all counters were individually re-tested with an LED [?]. 0.1% of counters  
 331 failed the LED tests and were therefore not used during the assembly of modules. The  
 332 assembly of modules was completed in June 2017, and it was then tested in June and July  
 333 2017 at the Proton Synchrotron experimental hall at CERN with a mixed particle beam  
 334 comprising mostly muons whose momenta could be selected between 0.5 and 5 GeV/c. An  
 event display from the summer 2017 tests is shown in Figure 14.

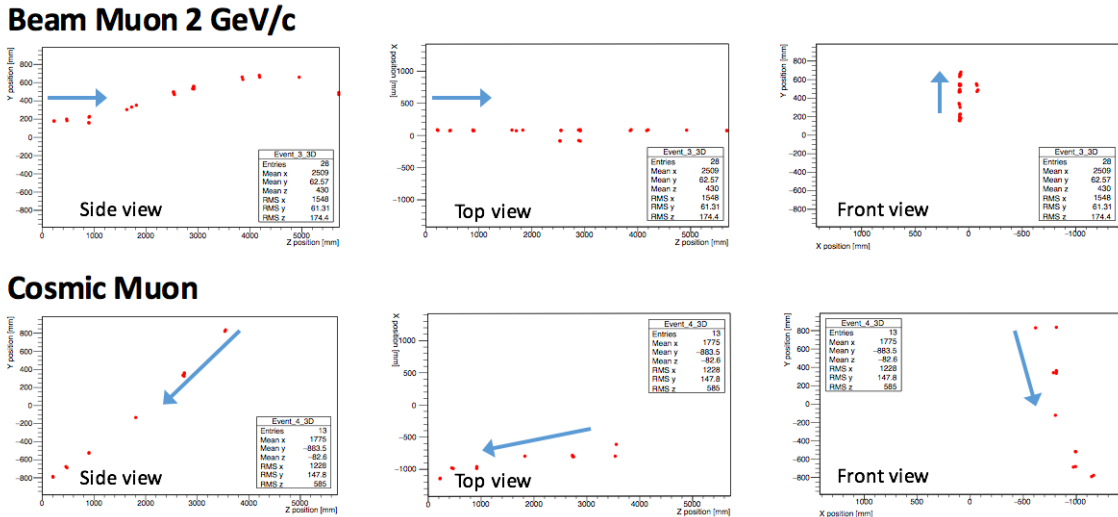


Figure 14: Comparison of a beam muon and cosmic muon in the three different geometrical projections of the detector. The beam impinges on the detector from the left. The arrows indicate the direction of travel of these muons. The direction of the cosmic muon is inferred from timing information.

335

336 **2.4 Side muon range detector**

337 Two Side-MRD modules for tracking secondary particles from neutrino interactions will be  
338 installed in 2018. Each Side-MRD module is composed of 11 steel plates and 80 scintillator  
339 slabs. The slabs are arranged as 10 layers installed in the 13 mm gaps between the 30 mm  
340 thick plates. Each steel plate size is 30 mm  $\times$  1610 mm  $\times$  1800 mm. Total module size is  
341 2236 mm  $\times$  1630 mm  $\times$  975 mm as shown in Figure 15 (left), weight is  $\sim$ 8.5 tonne.

342 Scintillator bars were manufactured by Uniplast company in Vladimir, Russia. Polystyrene  
343 based scintillators were extruded with thickness of 7 mm, then cut to the size of 7  $\times$  200  $\times$   
344 1800 mm<sup>3</sup>. Dopant composition is 1.5% PTP and 0.01% POPOP. Scintillator surface was  
345 etched by a chemical agent to form a white diffuse layer with excellent reflective perfor-  
346 mance. Ideal contact between the scintillator and the reflector raises the light yield up  
347 to 50% comparing to an uncovered scintillator. A sinusoidal groove was milled along the  
348 scintillator to provide uniform light collection over the whole scintillator surface. WLS Y11  
349 Kuraray fiber of 1 mm diameter was glued with an optical cement EJ-500 in the S-shape  
350 groove as shown in Figure 15(right). A minimum bending radius of 30 mm was used to  
351 ensure the the Kuraray S-type fibers remained within specification. Both ends of the fiber  
352 were glued into optical connectors which were themselves attached to the scintillator and  
353 provide an interface to SiPMs, Hamamatsu MPPC S13081-050CS(X1).

354 Scintillators for the Side-MRD modules were assembled at INR in Russia, and shipped  
355 to Japan in July 2017. The light yield for each scintillator was measured with cosmic  
356 rays at INR and at YNU in Japan after delivery.  $LY_1$  and  $LY_2$  are light yields measured  
357 at both ends of the counter. The light yield asymmetry between the ends calculated as  
358  $100\% \times \frac{LY_1 - LY_2}{LY_1 + LY_2}$ . After tests at INR we selected 324 counters from measured 332 ones with  
359 the mean light yield of 45 p.e./MIP ( $LY_1 + LY_2$ ) and the asymmetry value less than 10  
360 %. The measurements at YNU yielded the average total light yield of about 40 p.e./MIP  
361 which varies in range from 32 to 50 p.e./MIP (Figure 16 (left)). Only two counters showed  
362 relatively high asymmetry close to 25 % as shown in Figure 16 (right). Using the results of  
363 the quality assurance test we selected 320 scintillator counters for the Side-MRD modules.

364 We also measured the time resolution for a combination of four counters piled one  
365 upon another. The average result for four counters is  $\sigma_T = 1.04$  ns. The resolution of  
366 combination of 2, 3, 4 counters is measured to be 0.79 ns, 0.66 ns and 0.58 ns, respectively.

367  
368 Construction of the Side-MRD modules is scheduled from November 2017 at Yokohama  
369 National University. They will then be transported to J-PARC for installation on the B2  
370 floor of the T2K near detector hall.

371 Same electronics as the WAGASCI modules (see Sec. 2.1.2) are used for the Side-MRD  
372 modules.

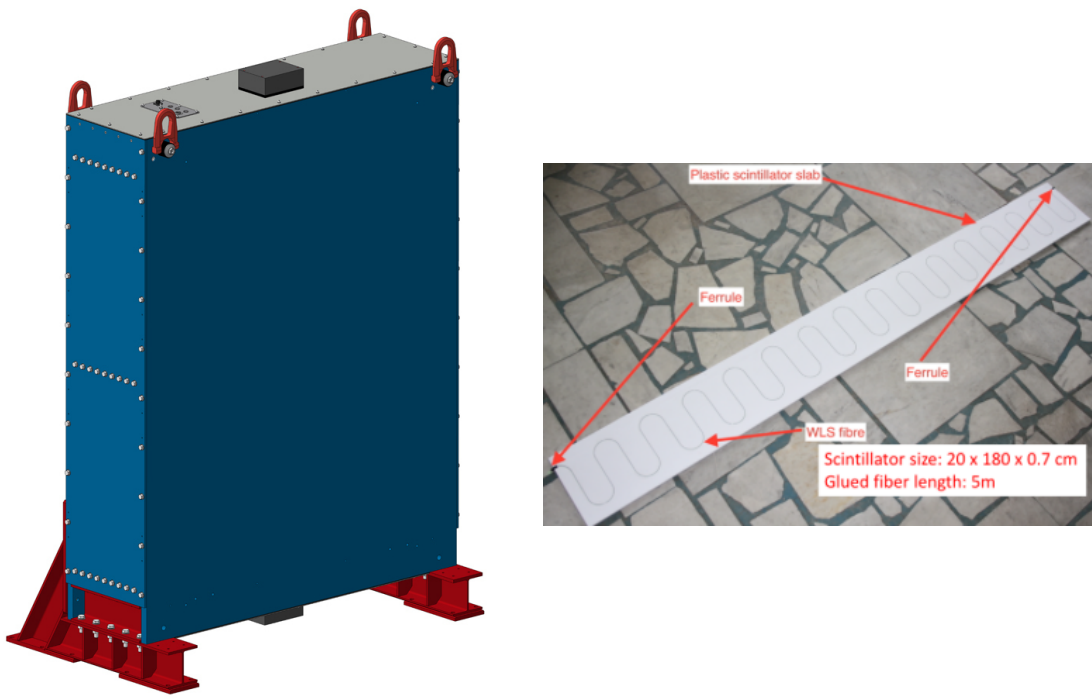


Figure 15: Left :Side-MRD module. Right: Scintillator bar of the Side-MRD modules.

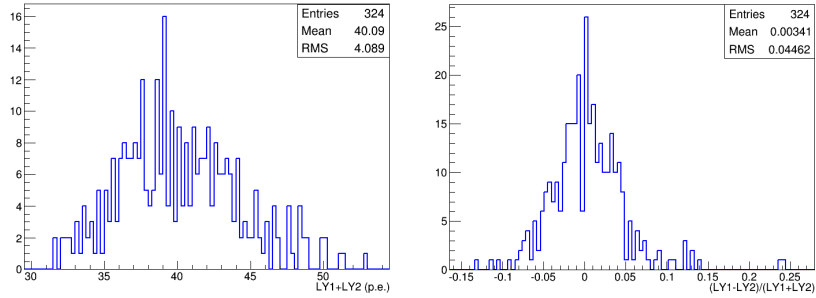


Figure 16: Total light yield distribution (left) and light yield assymetry (right) measured at YNU.

### 3 Physics goals

We will measure the differential cross section for the charged-current (CC) interaction on H<sub>2</sub>O and Hydrocarbon(CH)). The water-scintillator mass ratio of the WAGASCI module is as high as 4:1 and the high purity measurement of the cross section on H<sub>2</sub>O is possible. One experimental option is to remove water from one of the two WAGASCI modules. The water-out WAGASCI module will allow to measure pure-CH target interactions with very low momentum-threshold for protons. This will also allow this CH interaction background to be subtracted from the water-in target measurement. Another option is to add the T2K proton module which is fully made of plastic scintillators. It will allow the high statistics comparison of cross section between H<sub>2</sub>O and CH and also comparison with the ND280 measurement. The actual configuration will be optimized with detailed MC simulation by 2018 Summer.

Our setup allows the measurements of inclusive and also exclusive channels such as 1 $\mu$ , 1 $\mu$ 1p, 1 $\mu$ 1 $\pi^{\pm}$ np samples, the first two of which are mainly caused by the quasi-elastic and 2p2h interaction and the latter is mainly caused by resonant or coherent pion production and deep elastic scattering. In general, an accelerator produced neutrino beam spectrum is wide and the energy reconstruction depends upon the neutrino interaction model. Therefore, recent neutrino cross section measurements including those from T2K are given as a flux-integrated cross section rather than cross sections as a function of the neutrino energy to avoid the model dependency. We can provide the flux-integrated cross section. In addition, by combining our measurements with those from ND280, model-independent extraction of the cross section for narrow energy spread becomes possible. This method was demonstrated in [1] and also proposed by E61 (NUPRISM) experiment.

396 **3.1 Expected number of events**

397 Expected number of CC neutrino events remaining after the event selections was evaluated  
398 with simulation. Details are described in Sec. 5. In neutrino-mode, 5,400, 1,100 and 3,800  
399 events are expected for the water-in WAGASCI module, the water-out WAGASCI module  
400 and the INGRID proton module with  $5 \times 10^{20}$  POT. Among 5,400 events for the water-in  
401 WAGASCI module, 78 % are interactions on H<sub>2</sub>O. In the antineutrino-mode, 2,240, 400  
402 and 1,500 CC antineutrino events are expected for the water-in WAGASCI module, the  
403 water-out WAGASCI module and the INGRID proton module with  $5 \times 10^{20}$  POT. Among 2,  
404 2,240, 74 % are interactions on H<sub>2</sub>O. The wrong-sign interactions in antineutrino-mode is  
405 561 events, but will be removed with 90 % or higher efficiency by Baby MIND.

406 **3.2 Pseudo-monochromatic beam by using different off-axis fluxes**

407 The off-axis method gives narrower neutrino spectrum, and the peak energy is lower for  
408 larger off-axis angle. There still remains a high energy tail mainly due to neutrinos from  
409 Kaon decay. The off-axis angle of the WAGASCI location is 1.5 degrees as opposed to  
410 2.5 degrees for ND280. Top two plots of Figure 17 show the energy spectra of fluxes and  
411 neutrino interaction events at these two different locations. Bottom two plots of Figure 17  
412 show the energy spectra of fluxes and neutrino interaction events obtained by subtraction  
413 of fluxes at ND280 and WAGASCI. We can effectively get two fluxes, from 0.2 GeV to  
414 0.9 GeV and 0.6 GeV and 2 GeV and measure flux-integrated cross section for these two  
415 fluxes. It should be noted that even though the statistical errors are drawn for each energy  
416 bin for the bottom right plot of Fig. 17, measurement results will be given as an integration  
417 across energies.

418 **3.3 Extraction of Cross sections**

The flux-integrated CC inclusive cross sections on H<sub>2</sub>O and CH are calculated from the  
number of selected events with background subtraction and efficiency correction

$$\sigma_{CC} = \frac{N_{sel} - N_{BG}}{\phi T \epsilon},$$

419 where  $N_{sel}$  is the number of selected events from the real data,  $N_{BG}$  is the number of  
420 contaminated background events,  $\phi$  is the integrated  $\nu_\mu$  flux,  $T$  is the number of target  
421 nucleons, and  $\epsilon$  is the detection efficiency for signal estimated by MC simulation. The  
422 number of main background events is effectively estimated from side-band samples. The  
423 CH interaction background for the H<sub>2</sub>O measurement is estimated from the measurement  
424 of the Water-out WAGASCI module and/or the proton module. The neutrino interaction  
425 background for the antineutrino measurement is estimated from the opposite-sign inter-  
426 actions selected by Baby MIND. The dominant error for the inclusive total cross section  
427 measurement is the uncertainty of the neutrino flux, which is ~9% now and is expected

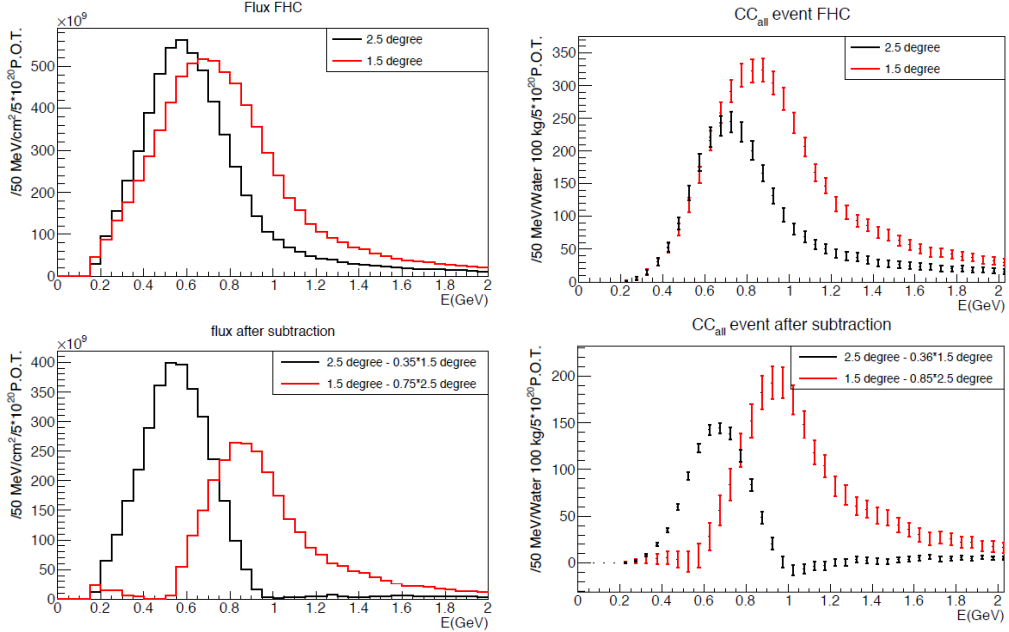


Figure 17: Energy spectra obtained by using different off-axis angle fluxes. Top two plots show the fluxes(left) and spectra of interaction events (right) for ND280 (off-axis 2.5 degree) and WAGASCI (off-axis 1.5 degree). Bottom two plots show the fluxes (left) and spectra of interaction events (right) obtained by subtraction of fluxes at ND280 and WAGASCI. The error bars represent the statistical error and those in the bottom right plot assume the statistical error for ND280 measurements are much smaller than those of the WAGASCI experiment.

428 to be reduced to  $\sim 6\%$ . Since the flux error is dominated by the normalization type error,  
429 the flux error can be significantly reduced for the relative comparison of the H<sub>2</sub>O and CH  
430 cross sections and the relative comparison of the ND280 and WAGASCI measurements.  
431 For example, T2K INGRID succeeded to determine the cross section ratio for CH and  
432 Fe with 3% precision[5]. For the exclusive and/or differential corss section measurements,  
433 statistical error would be dominant, size of which depending on the binning.

434 **3.4 Subjects WAGASCI can contribute**

435 Recent accelerator neutrino experiments use nuclear target e.g. organic scintillator, water  
436 and iron. So the interaction is largely affected by nuclear effects such as Fermi motion,  
437 correlated pairs of nucleons in nucleus (two particles-two holes, 2p2h), collective nuclear  
438 effects and final state interactions (FSI) of secondary particles in the nuclei after the initial  
439 neutrino interactions.

440 The main interaction type at the T2K energy (sub GeV) is the CC quasi-elastic (CCQE)  
441 interaction with nucleons inside nucleus. The energy is reconstructed from the lepton  
442 momentum assuming CCQE kinematics in T2K and other interactions would bias the  
443 reconstructed energy. Figure 18 shows how the reconstructed energy is affected. The 2p2h  
444 interactions mainly happen through the interaction with a correlated nucleons pair and also  
445 through the  $\Delta$  resonance interaction followed by pion-less decay. The 2p2h interactions  
446 are observed in electron scattering experiments [8] where the 2p2h events were observed  
447 in the gap between quasi-elastic region and pion-production region. Neutrino experiments  
448 have attempted to measure the 2p2h interactions, but so far there are only indicative  
449 results because the energy spectrum of the neutrino beam is wide and the precision of the  
450 event-by-event determination of the neutrino energy is not good nor suffered from bias. Our  
451 measurements, when combined with ND280 measurement, will give the cross section values  
452 for narrow energy-spread fluxes and give insight for such interactions. Another efficient  
453 way to investigate the 2p2h interaction is direct measurement of proton tracks with low  
454 momentum threshold and wide acceptance. Figure 19 left plot shows proton multiplicities  
455 for the CCQE events and 2p2h events. Figure 19 right plot shows opening angles of two  
456 proton-tracks for the events having two protons. The water-out WAGASCI can provide  
457 good sample for the 2p2h interaction search because its low density medium enables the  
458 detection of low momentum protons in side acceptance.

459 There are various models which describe the collective nuclear effects [9]. The wide  
460 acceptance of the WAGASCI experiment will provide information complementary to ND280  
461 and will play important role to select and tune models.

462 T2K is starting to use  $\nu_e$  CC1 $\pi$  samples at the far detector to increase the statistics.  
463 One of the biggest uncertainty of the CC1 $\pi$  sample comes from the final state interac-  
464 tions of pions in the nuclei after the initial neutrino interactions because they change the  
465 multiplicity, charge and kinematics of the pions. The multi-pion production events can  
466 be migrated into the CC1 $\pi$  sample due to the FSIs, and they become backgrounds. The

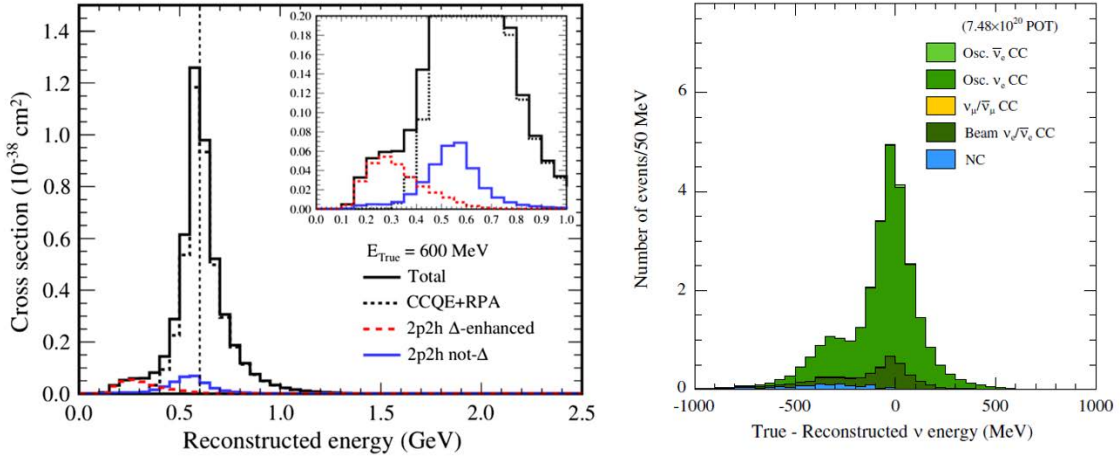


Figure 18: Left: reconstructed neutrino energy for CCQE and 2p2h interactions of 600 MeV muon neutrinos on  $^{12}C$  simulated with a mode. Right: difference between true and reconstructed energy of the  $\nu_e$  CCQE-like sample. The energy is reconstructed from the lepton momentum assuming the kinematics of the CCQE interaction. Both plots from [2]

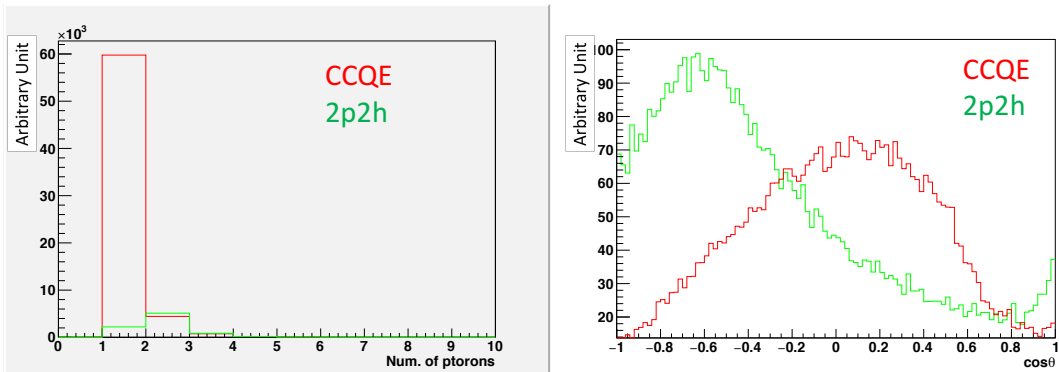


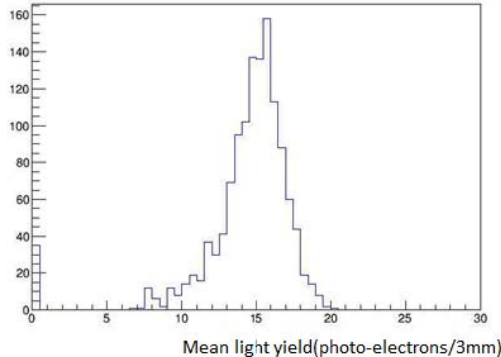
Figure 19: Proton multiplicities (left) and opening angles between two proton tracks (right) for CCQE events and 2p2h events. The final-state interaction is taking into account.

467 WAGASCI module has a capability to distinguish the pion track and proton track from  
468  $dE/dx$ , so WAGASCI can provide the CC $1\pi$  cross section with low momentum threshold  
469 and wide acceptance for pion tracks.

## 470 4 Status of J-PARC T59 experiment

471 We had submitted a proposal of a test experiment to J-PARC in April 2014 to test a new  
472 detector with a water target, WAGASCI, at the neutrino monitor hall, and the proposal  
473 was approved as J-PARC T59. The project contains the side and downstream muon range  
474 detectors as well.

475 The first WAGASCI module has been constructed in 2016 and installed at the on-axis  
476 position in front of the T2K INGRID detector for the commissioning and the first cross  
477 section measurement as a part of the T2K experiment. The INGRID electronics boards are  
478 used to read the signal. The light yield measured with muons produced by the interaction  
479 of neutrinos in the hall wall, shown in Figure 20, is sufficiently high to get a good hit  
efficiency. A track search algorithm based on the cellular automaton has been developed



480  
481 Figure 20: Light yield for muons produced by the interaction of neutrinos in the hall wall.  
482 Average light yields for each channel are plotted.

483 using the software tools from T2K INGRID. Examples of observed events are shown in  
484 Figure 21. The tracking efficiency in a 2-dimensional projected plane was evaluated by  
485 comparing the reconstructed track in the WAGASCI module and the INGRID module,  
486 and is shown in Figure 22. Note that that the tracking efficiency for high angle ( $> 70$  deg)  
487 is not evaluated because of the acceptance of the INGRID module, not because of the  
488 limitation of the WAGASCI module.

489 In 2017 Autumn, the construction of the second WAGASCI module and the dedicated  
490 electronics board were completed. The module and the electronics were install on the B2

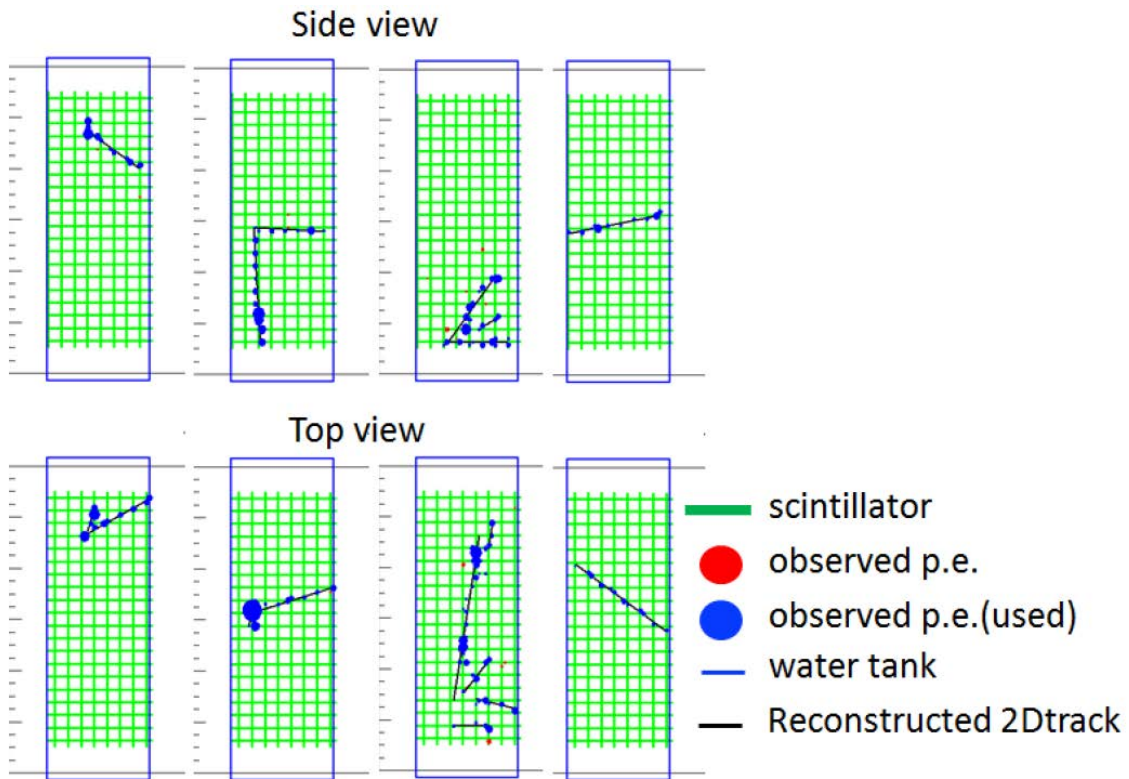


Figure 21: Example event displays of the WAGASCI module at on-axis. The reconstructed tracks are overlaid.

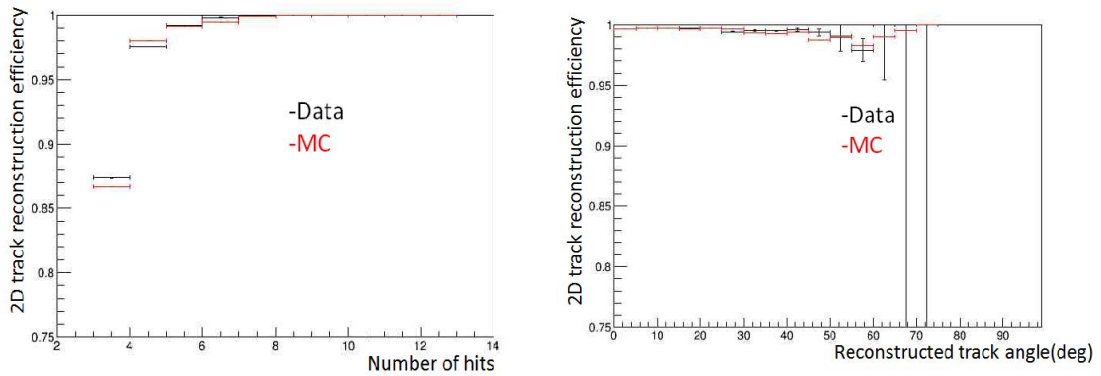


Figure 22: 2D track reconstruction efficiency as a function of number of hits (left) and track angle (right). Here the track angle is the one reconstructed by the INGRID module.

489 floor together with the T2K proton module and the INGRID module as shown in Figure 23.  
 490 The proton module is to be used as the entering muon veto and also for the comparison  
 491 of interaction between CH and Water. The INGRID module will act as the muon detector  
 492 for this period but due to its limited acceptance angle this is only a temporary measure.  
 493 The detector was commissioned and since October has been in operation taking data with  
 494 the T2K antineutrino beam.

495 The production of the components of the side muon range detectors has been completed  
 496 and now the detectors are being assembled at the Yokohama National University. These  
 497 detectors will be installed between January and June 2018, when T2K is not running.

498 The Baby MIND detector was transported from CERN to Japan in December, 2017.  
 499 It will be installed and commissioned in Jan.-Feb. 2018 and T59 will take the neutrino-  
 500 induced muon data in April and May.

## 501 5 MC studies

### 502 5.1 Simulation setup

503 The expected number of neutrino events in the water-in Wagasci detector is predicted by  
 504 Monte Carlo simulations. Neutrino beam flux at the detector location is simulated by  
 505 T2K neutrino flux generator, JNUBEAM. Neutrino interactions with target materials are  
 506 simulated by a neutrino interaction simulator, NEUT. Detector responses are simulated  
 507 using GEANT4-based simulation.

508 The detector geometry in the simulation so far is different from the actual setup as  
 509 shown in Figure 24. The active neutrino target region consists of four WAGASCI modules.

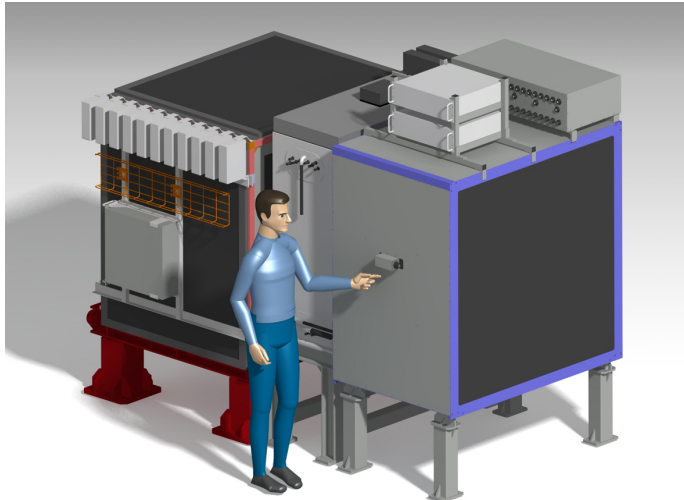


Figure 23: J-PARC T59 detector configuration in October 2017.

510 The size of the WAGASCI module is same as the actual one: 1000 mm  $\times$  1000 mm in the  
 511 x and y directions and 500 mm along the beam direction (z-direction). Two Side-MRD  
 512 modules are installed either side of the Wagasci modules. Each Side-MRD module consists  
 513 of ten iron plates whose dimension is 30 mm (thickness)  $\times$  2000 mm (height)  $\times$  3200 mm  
 514 (width). The distance between the Side-MRD modules and WAGASCI modules is 800  
 515 mm. The downstream-MRD is equivalent to the Baby-MIND, but without the magnetic  
 516 field. It consists of thirty iron plates whose dimension is 30 mm (thickness)  $\times$  2000 mm  
 517 (height)  $\times$  4000 mm (width). The distance between the downstream-MRD modules and  
 518 WAGASCI modules is 800 mm. Update of the study with the actual geometry is now  
 519 underway.

520 To simulate the signal, the energy deposit inside the scintillator is converted into the  
 521 number of photons. The effects of collection and attenuation of the light in the scintillator  
 522 and the WLS fiber are simulated, and the MPPC response is also taken into account. The  
 523 light yield is smeared according to statistical fluctuations and electrical noise.

## 524 **5.2 Charged-current event selection**

525 Tracks are reconstructed in two-dimensional planes in each sub-detector. Then, track  
 526 matching among the sub-detectors and three-dimensional track reconstruction are per-  
 527 formed. These analysis tools have been developed from the software tools by the T2K  
 528 INGRID and in mature stage already.

529 The events are selected as follows. The starting point of the track is required to be

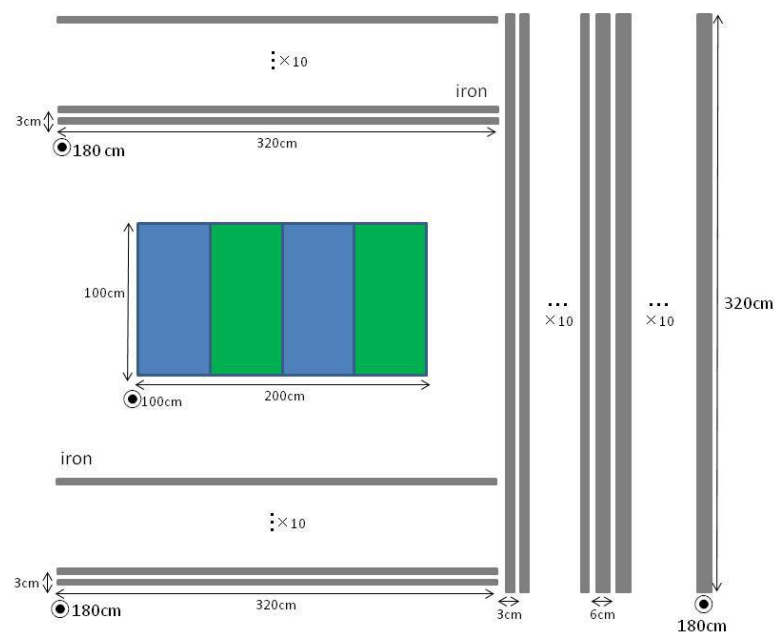


Figure 24: Geometry of the detectors in the Monte Carlo simulation.

530 50 mm away from the edge of the WAGASCI module. This is to remove the background  
 531 from the outside. The longest track has to penetrate more than one (five) iron plates in  
 532 Side-MRD modules (Baby-MIND). This cut select a muon track and rejects backgrounds  
 533 from NC and neutral particles. Then, in order to determine the muon momentum, it is  
 534 required that the longest track stops in MRDs (Side-MRD modules and Baby-MIND) or  
 535 penetrate all iron plates.

536 Table 1 shows numbers of the selected events in one water-in WAGASCI module after  
 537 the event selection. We expect 4,239 (1,666) events from charged-current interaction on  
 538  $H_2O$  with  $5 \times 10^{20}$  POT in (anti)neutrino-mode with one water-in WAGASCI module.  
 539 The purity, when interactions on CH is counted as background, is 78% for the neutrino-  
 540 mode. There is a significant contamination from the wrong-sign (neutrino) interaction for  
 541 antineutrino-mode, however, we expect that it will be removed with efficiency higher than  
 90% by Baby MIND.

Table 1: Expected number of the selected neutrino-candidate events in one water-in WAGASCI module with  $5 \times 10^{20}$  POT in each of neutrino-mode and antineutrino-mode. Note that the wrong sign component will be reduced by one order by applying the charge selection by Baby MIND.

	CC on $H_2O$	NC on $H_2O$	Interaction on CH	wrong sign interaction
$\nu$ -mode	4239	107	1087	(negligible)
anti- $\nu$ -mode	1666	14	560	(561)

542  
 543 Table 2 and 3 summarize contributions classified by the interaction types and final state  
 topologies for the selected charged current-interaction events, respectively.

Table 2: Interaction types for the selected charged-current events.

	CCQE	2p2h	CC resonant $\pi$	CC-DIS
$\nu$ -mode	48.4 %	9.7 %	27.1 %	14.7 %
anti- $\nu$ -mode	57.1 %	8.2 %	17.3 %	17.3 %

Table 3: Final state topologies for the selected charged-current events.

	CC0 $\pi$	CC1 $\pi$	CC2 $\pi$	CCn $\pi$
$\nu$ -mode	67.4 %	20.9 %	3.0 %	8.7 %
anti- $\nu$ -mode	79.5 %	16.3 %	1.2 %	3.0 %

544

545     Figure 25 shows the reconstructed angles of the longest tracks in the selected events in  
 546 the neutrino-mode and the anti-neutrino mode. Figure ?? shows the iron plane numbers  
 547 in Side-MRD and Baby-MIND corresponding to the end points of the longest tracks in the  
 selected events in the neutrino-mode and the anti-neutrino mode.



Figure 25: The reconstructed angles of the longest tracks in the selected events in the neutrino-mode (left) and the antineutrino-mode (right).

548

### 549    5.3 Standalone WAGASCI-module tracking performance

550    The previous section has described the inclusive charged-current event selection using the  
 551 Muon Range detectors. A muon is identified by requiring one track to penetrate multiple  
 552 planes of the MRD's. For the WAGASCI configuration described in Sec. 5.1, only 7% of  
 553 the muons are stopped in one of the WAGASCI modules. This proportion increases to  
 554 53% for pions and 73% for protons produced by neutrino interactions. Figure 27 shows the  
 555 momentum distribution of these daughter particles as well as for the sub-sample stopped  
 556 in one of the WAGASCI modules. For the measurement of the neutrino interaction final  
 557 states, tracks of charged pions, protons and low-momentum ( $p_\mu < 300$  MeV/c) muons have  
 558 to be reconstructed by the WAGASCI module. Therefore, the standalone tracking abilities  
 559 of the WAGASCI module, especially momentum threshold, is important for the exclusive  
 560 interaction measurements.

561    Here we present the result of the study based on an original study done for the T2K  
 562 ND280 upgrade with some modifications. Though the cell size is similar to the WAGASCI  
 563 configuration, the external dimensions are different (1864 mm  $\times$  600 mm  $\times$  1300 mm). We  
 564 present the results which are less affected by the difference of the external dimensions.

565    A simplified criteria , but representing conditions for the WAGASCI module tracking,  
 566 are applied to evaluate the reconstruction performance of the WAGASCI module. The  
 567 fiducial volume is chosen as the inner cube of the module which surfaces are 4 scintillator  
 568 space = 100 mm distant from the module external surfaces. A track is reconstructed if:

- 569    • The track is long enough and has at least 2 hits in both of two views (XZ, YZ). In

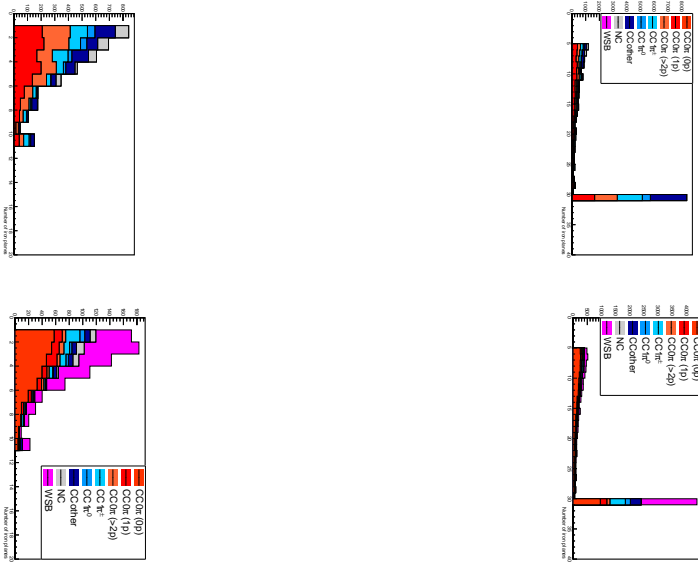


Figure 26: Iron plane numbers in Side-MRD (left) and Baby-MIND (right) corresponding to the end points of the longest tracks in the selected events in the neutrino-mode (top) and the antineutrino-mode (bottom).

570           the pure longitudinal or transverse going tracks, it corresponds to the track length  
 571           of 100 mm.

- 572           • The track shall not be superimposed with longer tracks in both of two views. The  
 573           superposition criterion is estimated with the distance inter-tracks (DIT) which cor-  
 574           responds to the orthogonal distance between two tracks at the ending point of the  
 575           shortest one (see Figure 28). The DIT should be higher than  $4 \times$  scintillator width  
 576           ( $=100$  mm) for the shorter track not to be superimposed with the longer track.

577       **5.3.1 Expected performance of the water-in WAGASCI module**

578       Figures 29 shows the expected track reconstruction efficiency obtained with the criteria  
 579       above. Table 4 summarizes the reconstruction efficiencies and the reconstruction momen-  
 580       tum thresholds. This threshold is defined as the momentum under which the reconstruc-  
 581       tion efficiency falls under 30%. The thresholds for muon and pion are 150 MeV/c. The lower  
 582       pion and proton efficiencies (respectively 52% and 26%) are due to lower momentum and  
 583       also due to the secondary interaction. Efficiencies of each particle type tend to decrease in  
 584       the backward region due to lower particle momenta. However, for a fixed momentum value,

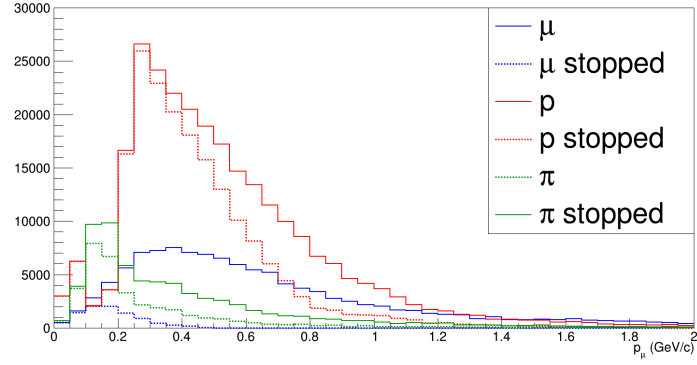


Figure 27: Momentum distribution of particles in WAGASCI (plain) and corresponding distributions only for particles stopping in the WAGASCI module (dashed).

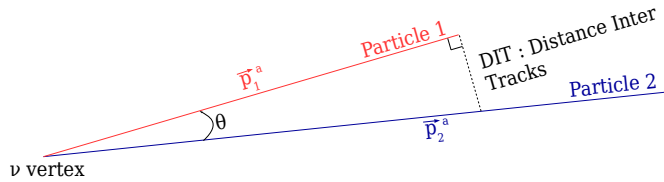
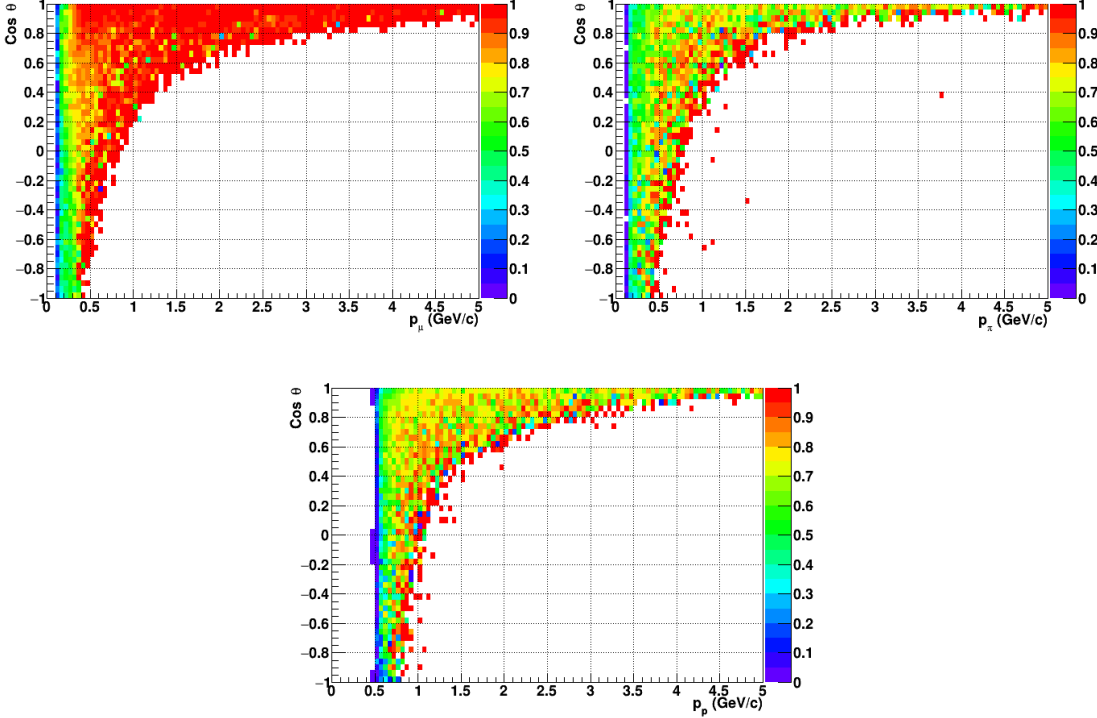


Figure 28: Definition of the distance inter tracks.

Table 4: Reconstruction efficiency and momentum threshold for muons, pions and protons. The threshold is defined as the momentum under which the reconstruction efficiency falls under 30%.

	$\mu$	$\pi$	p
Reconstruction Efficiency	79%	52%	26%
Momentum threshold	150 MeV/c	150 MeV/c	550 MeV/c

585 the reconstruction efficiency do not strongly depend on the angle thanks to the WAGASCI  
grid structure.



586 Figure 29: Reconstruction efficiency of muons (left), charged pions (right) and protons  
(bottom) in the WAGASCI water-module as a function of the particles momenta and  
angles.

586

### 587 5.3.2 Expected performance of the water-out WAGASCI module

588 One experimental option is to remove water from one of the two WAGASCI modules. The  
589 detector is fully active and has a 3 mm spatial resolution (scintillator thickness) which  
590 create an ideal detector to reconstruct and identify hadrons, and study 2p2h interaction.  
591 The same reconstruction criteria as in Sec. 5.3.1 are applied for the water-out module.  
592 Figure 30 shows the comparison between the water-in and the water-out reconstruction  
593 efficiencies for muon, pions and protons. 90% of the muons and 87% of the pions are  
594 reconstructed, while 70% of the protons are even reconstructed. It allows to low down the  
595 proton threshold to 250 MeV/c (see Table 5). The water-out module offers interesting  
596 possibilities to study 2p2h interaction since 70% of the protons are reconstructed.

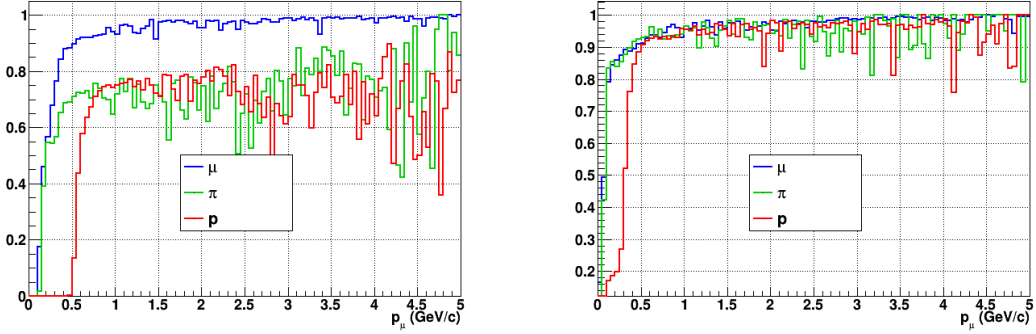


Figure 30: Reconstruction efficiency for muons, pions and protons in the water-in (left) and water-out (right) modules.

Table 5: Reconstruction efficiency, proportions of  $\mu$ -like and non  $\mu$ -like and momentum threshold for muons, pions and protons for the water-out module. The threshold is defined as the momentum under which the reconstruction efficiency falls under 30%.

	$\mu$	$\pi$	p
Reconstruction Efficiency	90%	87%	70%
Momentum threshold	50 MeV/c	50 MeV/c	250 MeV/c

597 **6 Schedule**

598 We would like to start a physics data taking from T2K beam time after the summer  
599 shutdown in 2018. By then, commissioning and tests of the detectors will be completed  
600 in J-PARC T59. The experiment can run parasitically with T2K, therefore we request no  
601 dedicated beam time nor beam condition as discussed in the following section.

602 **7 Requests**

603 **7.1 Neutrino beam**

604 The experiment can run parasitically with T2K, therefore we request no dedicated beam  
605 time nor beam condition. As data taking periods, we request the ‘nominal’ T2K one-year  
606 operation both for the neutrino beam and the antineutrino beam. The T2K has been  
607 requesting  $0.9 \times 10^{21}$  POT/year and actually accumulating about  $0.7 \times 10^{21}$  POT/year in  
608 recent years. For each year, starting from the Autumn, T2K is running predominantly in  
609 the neutrino mode or in the antineutrino mode. Our request is to have one-year neutrino-  
610 mode data and another one-year antineutrino mode data assuming that the POT for the  
611 fast extraction in each year is more than  $0.5 \times 10^{21}$  POT.

612 **7.2 Equipment request including power line**

613 We request the followings in terms of equipment on the B2 floor:

- 614 • Site for the WAGASCI modules, Side-MRD modules and BabyMIND and their elec-  
615 tronics system on the B2 floor of the near detector hall (Figure 2 and 3).
- 616 • Anchor points (holes) on the B2 floor to secure the WAGASCI modules, Side-MRD  
617 module and Baby-MIND, detailed floor plans to be communicated in a separate  
618 document.
- 619 • Power line for the magnets in Baby-MIND: 400 V tri-phase 48-to-62 Hz, capable of  
620 delivering 12 kW. We have a wish for the magnet power line to be installed and  
621 available to us by beginning of March 2018.
- 622 • Electricity for electronics and water circulation system, 3 kW, standard Japanese  
623 electrical sockets.
  - 624 1. Online PCs: 2.1 kW
  - 625 2. Electronics: 0.7 kW
  - 626 3. Water sensors: 1 kW
- 627 • Air conditioner for cooling heat generation at Baby-MIND magnets, online PCs and  
628 electorronics

- 629       • Beam timing signal and spill information  
630       • Network connection

631       The infrastructure for much of the above exists already. Exceptions are the power line  
632       for the magnet and the electronics and holes in the B2 floor to anchor the detector support  
633       structures.

634       After this WAGASCI experiment, Baby MIND and Side-MRD's will remain if approved  
635       by J-PARC, and be used as common platforms of future neutrino experiments using the  
636       J-PARC neutrino beam.

## 637       References

- 638       [1] K. Abe et al. Measurement of the muon neutrino inclusive charged-current cross  
639       section in the energy range of 13 GeV with the T2K INGRID detector. *Phys. Rev.*,  
640       D93(7):072002, 2016.
- 641       [2] K. Abe et al. Measurement of neutrino and antineutrino oscillations by the T2K  
642       experiment including a new additional sample of  $\nu_e$  interactions at the far detector.  
643       *Phys. Rev.*, D96(9):092006, 2017.
- 644       [3] M. Antonova et al. Baby MIND Experiment Construction Status. In *Prospects in*  
645       *Neutrino Physics (NuPhys2016) London, London, United Kingdom, December 12-14,*  
646       2016, 2017.
- 647       [4] K. Nitta et al. The k2k scibar detector. *Nucl. Instrum. Meth. A*, 535:147, 2004.
- 648       [5] K. Abe et al. (T2K Collaboration). Measurement of the inclusive  $\nu_\mu$  charged current  
649       cross section on iron and hydrocarbon in the t2k on-axis neutrino beam. *Phys. Rev.*  
650       D, 90:052010, 2014.
- 651       [6] F. Magniette F. Gastaldi, R. Cornat and V. Boudry. A scalable gigabit data acquisition  
652       system for calorimeters for linear collider. *proceedings of TIPP2014*, page PoS 193,  
653       2014.
- 654       [7] J. Fleury, S. Callier, C. de La Taille, N. Seguin, D. Thienpont, F. Dulucq, S. Ahmad,  
655       and G. Martin. Petiroc and Citiroc: front-end ASICs for SiPM read-out and ToF  
656       applications. *JINST*, 9:C01049, 2014.
- 657       [8] M. B. Barbaro J. A. Caballero T. W. Donnelly G. D. Megias, J. E. Amaro. Inclusive  
658       electron scattering within the susav2 meson-exchange current approach. *Phys. Rev.*  
659       D, 94:013012, 2016.
- 660       [9] M. Valverde J. Nieves, J. E. Amaro. Inclusive quasi-elastic neutrino reactions. *Phys.*  
661       *Rev. C*, 70:055503, 2004.

- 662 [10] Yu. G. Kudenko, L. S. Littenberg, V. A. Mayatsky, O. V. Mineev, and N. V. Ershov.  
663       Extruded plastic counters with WLS fiber readout. *Nucl. Instrum. Meth.*, A469:340–  
664       346, 2001.
- 665 [11] O. Mineev, Yu. Kudenko, Yu. Musienko, I. Polyansky, and N. Yershov. Scintillator  
666       detectors with long WLS fibers and multi-pixel photodiodes. *JINST*, 6:P12004, 2011.
- 667 [12] Etam Noah et al. Readout scheme for the Baby-MIND detector. *PoS*, Pho-  
668       toDet2015:031, 2016.
- 669 [13] Omega. Spiroc 2 user guide. 2009.